To be submitted to the Astrophysical Journal

Evidence of the FIP effect in the coronae of late-type giants

David García-Alvarez, Jeremy J. Drake, B. Ball, LiWei Lin, Vinay L. Kashyap

[1]*Harvard-Smithsonian CfA,*
60 Garden Street,
Cambridge, MA 02138

ABSTRACT

β Cet, 31 Com and μ Vel represent the main stages through which late-type giants evolve during their lifetime (the Hertzsprung gap (31 Com), the rapid braking zone (μ Vel) and the core helium burning "clump" phase (β Cet)). An analysis of their high resolution *Chandra* X-ray spectra reveals similar coronal characteristics in terms of both temperature structure and element abundances for the more evolved stars (μ Vel and β Cet) with slight differences for the 'younger' giant (31 Com). The coronal temperature structure of 31 Com is significantly hotter showing a clear peak while β Cet and μ Vel show a plateau. β Cet and μ Vel show evidence for a FIP effect in which coronae are depleted in high FIP elements relative to their photospheres by a factor of ~ 2. In contrast, 31 Com is characterized by a lack of FIP effect. In other words, neither depletion nor enhancement relative to stellar photospheric values is found. We conclude that the structural changes during the evolution of late-type giants could be responsible for the observed differences in coronal abundances and temperature structure. In particular, the size of the convection zone coupled with the rotation rate seem obvious choices for playing a key role in determining coronal characteristics.

Subject headings: stars: abundances — stars: activity — stars: coronae — stars: giants — Sun: corona — X-rays: stars

1. Introduction

The solar coronal abundance anomaly commonly known as the "FIP Effect" (or First Ionization Potential Effect), in which low first ionization potential (FIP) elements (e.g.; Si,

Fe, Mg) appear enhanced by average factors of 3-4, was already known by the time the first observational clues to similar abundance anomalies in stellar coronae were uncovered in the 1990's (e.g.; Feldman 1992). These clues came from low resolution soft X-ray spectra (*GINGA, ASCA, BeppoSAX*), together with moderate resolution extreme ultraviolet (EUV) spectra obtained by the Extreme Ultraviolet Explorer (EUVE). The early stellar studies found evidence for a solar-like FIP Effect in some stars, but for the more active stars the abundances pointed toward metal paucity rather than enhancement (Drake et al. 1994a; White et al. 1994).

The last four years—the beginning of the *Chandra* and *XMM-Newton* era— have seen early hints of abundance anomalies fleshed out into an interesting array of diverse abundance patterns in which active stars appear to show signs not only of low FIP element depletion, but also of high FIP element enhancements. Studies of solar-like active stars confirm the suspicions engendered by earlier work (e.g.; Drake et al. 1995) that a transition from a metal-depleted to a metal-rich corona occurs as the activity decreases (Güdel et al. 2002); this is now better characterised as a change from an apparently "inverse FIP effect" to a FIP effect. Audard et al. (2003) showed a similar transition from an inverse FIP effect to the absence of an obvious FIP effect for RS CVn binary stars with decreasing activity. Drake et al. (1995), Raassen et al. (2002) and Sanz-Forcada et al. (2004) showed that coronal abundances can also be similar to that of its underlying photosphere. Sanz-Forcada et al. (2004) also presented evidence of possible variation in coronal metal abundance relative to the temperature of the emitting plasma.

For some years we have argued (e.g., Drake 2003, and earlier references therein) that coronal abundances, when better understood, might provide new and powerful diagnostics of the physical processes underpinning stellar coronae. The emerging patterns of coronal abundance anomalies are telling us something about the dynamical structure and heating of coronal plasma; the challenge is to learn to read these patterns. Aiming toward this goal, one question that arises is that of fine tuning of abundance patterns: how do the abundance anomalies in the late-type giants compare with those of solar-like and other active stars?

In low-mass ($M<1.5\,M_\odot$) solar-type stars the magnetic activity is thought to derive from a dynamo powered by convection and driven by stellar spin (e.g. Parker 1970). Thus extremes in activity and rotation are closely related. Moderate-mass giants ($M\sim3.0\,M_\odot$), with A and late B progenitors on the MS having no outer convection zone, cross into the cool half of the H-R diagram during their post-main-sequence phase as yellow giants. The magnetic activity of these stars experiences several stages as they evolve: the Hertzsprung-gap phase of relatively rapid rotation (Simon & Drake 1989); the "rapid braking zone" (Gray 1989) and the red giant branch (RGB) phase (Ayres et al. 1983). The latter includes the

ascent of the RGB, the helium ignition at its tip, and the return to the base of the RGB as core helium burning ("clump") stars. The rejuvenation of magnetic activity of more evolved "clump" giants is not well understood. Infusion of angular momentum at the base of the RGB (Simon & Drake 1989) and the rejuvenation of the dynamo by planet/brown dwarf accretion (Siess & Livio 1999) have been suggested as possible causes. Coronal characteristics and X-ray emission, triggered by the onset of efficient convection occurring while passing through the Hertzprung-gap, may change in response to evolutionary changes of the rotation and internal structure of the star (e.g.; deepening of the convection zone, rapid expansion of the stellar radius and photosphere cool down). Yellow giants are particularly interesting due to the relatively short time scales in which internal structure changes which might affect the corona and the coronal abundances take place (Ayres et al. 1998; Gondoin 1999).

In this paper, using *Chandra* High Energy Transmission Grating spectrograph (HETGS) observations, we present a comparative analysis of the coronal X-ray spectra of the active late-type giants β Cet, 31 Com and μ Vel with particular emphasis on their abundances. We first describe the three stars and briefly review earlier work (§2), then in §3 we report on the *Chandra* observations and data reduction. The methods used for a differential emission measure analysis together with results obtained are shown in §4. In §5 we discuss our results on the coronal abundances and temperature structure and report our conclusions in §6.

2. Program Stars

Our sample represents different giant evolutionary stages: the Hertzsprung gap (31 Com), the rapid braking zone (μ Vel) and the core helium burning "clump" phase (β Cet). β Cet, 31 Com and μ Vel are among the more active single G-type giant stars in the solar neighborhood, lying about two orders of magnitude brighter in X-rays than the average value for single G-giants (L_x=28.7, Maggio et al. 1990).

2.1. β Cet

The "clump" giant β Cet (HD 4128, HR 188) is a well-studied nearby G9.5 III star (29 pc, Perryman et al. 1997). Its main physical parameters are shown in Table 1. Several works have shown that β Cet has a photosphere metal-rich relative to solar (see Table 2). The enhancement of the C/N abundance ratio (C/N=+0.4, Lambert & Ries 1981) clearly shows that β Cet has undergone first dredge-up, placing it, based on the evolutionary time-scale arguments, in the He-burning clump (Ayres et al. 1995). β Cet is the brightest FUV

and X-ray source among the single clump giants. Smith & Dominy (1979) called attention to the abnormally large photospheric macroturbulence velocity ($4.2\pm0.2\,\mathrm{km\,s^{-1}}$), and suggested that this could be related to the UV and X-ray emission if such motions are dissipated as heat by shocks in the chromosphere and corona. Ayres et al. (2001) reported a 34-day EUVE pointing during which a series of coronal flares were observed. Those long-duration outbursts (several days) are like the extremes seen on RS CVn type binaries (Foing et al. 1994; García-Alvarez et al. 2003). An earlier 6-day observation showed a flat light curve (Ayres et al. 1994). Drake et al. (1994b), based on ASCA observations, estimated the coronal abundance of a number of elements obtaining an atmosphere Mg-rich and S, Fe, O, Ne and N-poor relative to solar photospheric values. Similar results were reported by Maggio et al. (1998) based on SAX observations.

2.2. 31 Com

31 Com (HD 111812, HR 4883) is a G0 III rapidly rotating ($P< 7\overset{d}{.}2$) star 94 pc away (Perryman et al. 1997). It has the bluest color (B-V=0.67) among the single G giants observed by *Einstein Observatory* (Maggio et al. 1990). 31 Com has evolved out of the MS and is probably crossing the Hertzprung-gap, as suggested by its location in the H-R diagram and by the high abundance of lithium (log N(Li)=2.7, Mallik et al. 2003). In this phase 31 Com has developed a convective subphotospheric layer and dynamo. Metallicity has been examinated by Gustafsson et al. (1974) and Taylor (1999), revealing a slightly metal-poor photosphere relative to solar (see Table 2). 31 Com was noted to have moderately weak Ca II H&K lines with reversals (Wilson 1966). Strassmeier et al. (1994) reported photospheric line profile deformations most likely caused by cool starspots. Ayres et al. (1998) suggested rotational modulation of highly extended chromospheric structures as an explanation of secular changes in the Lyα profile.

31 Com has been observed several times in X-rays: Einstein (Maggio et al. 1990), ROSAT (Pizzolato et al. 2000), ASCA (Ueda et al. 2001), XMM-Newton (Scelsi et al. 2004). It shows evidence for excess broadening in Fe XXI (Ayres et al. 2003) which would imply, if the excess broadening is rotational, that the corona is highly extended, contrary to the compact structures suggested by recent density estimates in a number of active coronal sources. Scelsi et al. (2004) determined the emission measure distribution and coronal abundances for 31 Com based on XMM-Newton observations (RGS and EPIC spectra). They suggested a corona dominated by isothermal magnetic loops.

2.3. μ Vel

μ Vel (HD 93497, HR 4216) first appeared in the literature more than 100 years ago (See 1897), though detailed studies of the star have been undertaken. It is a close (2" apart) visual double system (G5 III+dF; 36 pc away Perryman et al. (1997)) consisting of a late-type giant and a fainter companion. Ayres et al. (1999) concluded that the companion is a single mid-F dwarf thought to be relatively inactive compared with the primary, and thus it should not contribute significantly to the observed X-ray emission. We return to this in §4. Ayres et al. (1999) reported, based on a deep pointing by EUVE, a large flare on μ Vel with a long 1.5 day decay.

Burnashev (1983) suggested μ Vel has a slightly metal-poor photosphere relative to solar (Holweger 1979), [Fe/H]=-0.12. Based on comparison with the evolutionary tracks of Schaller et al. (1992), Ayres et al. (1999) derived an age for μ Vel of $\sim$350 Myr and classified it as being in the "rapid braking zone" discussed by Gray (1989) that begins at spectral type G0-G3. Here the C IV activity is seen to drop simultaneously with a decline in rotational velocity. The properties of μ Vel are also fairly similar to those of the X-ray bright clump giants β Ceti and Capella Aa, including a low lithium abundance (log N(Li)=0.4 Mallik et al. 2003). While it lies very slightly to the blue of the Schaller et al. (1992) core He-burning clump, the lack of surface C and N abundance measurements precludes a definitive classification of its exact evolutionary state. For the purposes of our study here, however, this exact classification is not critical and we tentatively adopt the rapid braking zone classification of Ayres et al. (1999).

3. Observations

The *Chandra* HETGS observation of β Cet, 31 Com and μ Vel were carried out in 2001 using the AXAF CCD Imaging Spectrometer (ACIS-S) in conjunction with the High-Energy Transmission Grating Spectrometer (HETGS). All the observations employed the detector in its standard instrument configuration. The observations are summarized in Table 3. Note that two observations 3 months apart were obtained for μ Vel.

Fig. 1 shows the *Chandra* X-ray spectra of β Cet, 31 Com and μ Vel in the wavelength range 3-27 Å which contains prominent lines of Ne, N, O, S, Si, Fe, Mg, Al and Na. The strongest lines are identified. The spectra of β Cet and μ Vel show a remarkable similarity of lines, both in terms of which lines are prominent, from H- and He-like ions and the broad range of charge states of Fe, and in their relative intensities. The spectrum of 31 Com, although similar to the other two stars, shows stronger O and Fe lines. We also observe that

in β Cet and μ Vel the Fe XVII resonance line at 15.01 Å is strongest, in 31 Com Ne X Lyα is strongest.

4. Analysis

Pipeline-processed (CXC software version 6.3.1) photon event lists were reduced using the CIAO software package version 3.0, and were analyzed using the IDL[1]-based PINTofALE[2] software suite (Kashyap & Drake 2000). The analysis we have performed consisted of line identification and fitting, reconstruction of the plasma emission measure distribution including allowance for blending of the diagnostic lines used, and finally, determination of the element abundances.

4.1. Photometry

Before commencing spectral analysis, we first checked for flare activity that could affect not only the shape of the differential emission measures (DEMs) but might also be accompanied by detectable changes in the coronal abundances of the plasma that dominate disk-averaged spectra (see, e.g. Ottmann & Schmitt 1996; Mewe et al. 1997; Ortolani et al. 1998; Favata & Schmitt 1999; Favata et al. 2000; Maggio et al. 2000; Güdel et al. 2001). Light curves for β Cet, 31 Com and μ Vel observations (including Obs ID1890 and Obs ID3410 hereafter) were derived excluding the 0th order, which could be affected by pileup, and instead considered just the dispersed photons. Events were then binned at 100s intervals. Fig. 2 shows the light curves for all the observations; note that all the light curves are relatively flat and devoid of significant flare activity. The companion of μ Vel is just discernible in the 0th order X-ray image as a slight elongation of the wing PSF. While the X-ray spectrum of this mid-F dwarf cannot be separated from that of μ Vel, it contributes only $\sim 1\%$ of the total counts and so its influence in the analysis will be completely negligible.

We conclude that β Cet, 31 Com and μ Vel observations are representative of the stars during times of quiescence, and therefore treat the observations in their entirety for the remainder of the analysis.

---

[1]Interactive Data Language, Research Systems Inc.

[2]Available from http://hea-www.harvard.edu/PINTofALE

4.2. Spectroscopy

The emission measure distribution and abundance analysis employed the CHIANTI database version 4.2 (Dere et al. 2001) and the ionization balance of Mazzotta et al. (1998), as implemented in the PINTofALE software package (Kashyap & Drake 2000). Spectral line fluxes for β Cet, 31 Com and μ Vel were measured by fitting modified Lorentzian or Moffat ("β profile") functions of the form:

$$f(\lambda) = a/(1 + (\frac{\lambda - \lambda_0}{\Gamma})^2)^\beta \tag{1}$$

where a is the amplitude and Γ a characteristic line width. For a value of $\beta = 2.4$, it has been found that this function represents the *Chandra* transmission grating instrumental profile to within photon counting statistics for lines of the order of a few 1000 counts or less (Drake 2004). In the case of blends, as in Ne IX-Fe XIX in which both spectral lines are blended, we have performed multi-component fitting in order to obtain the flux of each line.

While strong lines can be easily identified, the sum of weak lines, each of which can be undetectable, can produce a "pseudo-continuum". The true continuum level was set using the spectral regions 2.4-3.4, 5.3-6.3 and 20.4-21.4 Å, which we judged to be essentially "line-free", based on both visual inspection and the examination of radiative loss models. These continuum points were then used to normalize model continua computed using a test Differential Emission Measure taken from an analysis of a typical active star (AU Mic in this case, Drake et al. (2005)). In principle, the fluxes should be re-measured once the final DEM has been determined; in practise, there was little difference in the *shapes* of trial and final continuum models so that this additional iterative step was not required.

Table 4 shows the measured fluxes of the emission lines identified and used in this analysis. We have computed correction factors (CF) for line blends. The procedure identifies which lines, within the CHIANTI emission line database, are possible contaminants for each analysed line. The contaminants must lie within two sigma of the line center and have predicted intensity greater than a user-defined threshold. Gaussian profiles are used,for simplicity of computation, as an approximation to the true profiles of the contaminants. The differences compared with the Moffat profiles, used to measure the spectral line fluxes, are not significant. The CF are defined as follows:

$$CF = \frac{I(\lambda_i)}{I(\lambda_i) + \sum_{j \neq i} I(\lambda_j)} \tag{2}$$

where I(λ_i) = intensity of the line being contaminated by lines $j \neq i$. CF for line blends for the studied lines range from 0.73 to 0.99. The measured fluxes are then multiplied by the CF in order to obtain the "true" flux of each line.

4.3. Differential Emission Measure

Our basic set of diagnostics comprises the H-like/He-like resonance line flux ratios for the elements O, Ne, Mg, and Si, line ratios involving Fe XVII, Fe XVIII and Fe XXI resonance lines, and measurements of the continuum flux at points in the spectrum that are essentially free of lines (the same regions noted above with regard to spectral line intensity measurement). This set of lines include the brightest lines in stellar coronal spectra and are easily measured in essentially all well-exposed *Chandra* grating observations of stellar coronae, such that star-to-star variations in diagnostic lines used can be avoided.

While atomic data for the H-like and He-like resonance lines used here are expected to be reliable this is not necessary the case for the Fe lines, for which both ionization balance and level population computations are much more complex. Doron & Behar (2002) and Gu (2003) reported new Fe L-shell calculations indicating that rate coefficients for n→2 (3<n<5) transitions originating from 3s and 3p upper levels may differ from earlier calculations up to 50%. They emphasised the importance of including in the level populations the indirect processes of radiative recombination, dielectronic recombination (DR), and resonance excitation involving neighbouring charge states. However, the Fe XVII 15.01Å and Fe XVIII 14.21Å lines used here arise from $3d$ upper levels which the calculations indicate are not significantly affected by these processes. Gu (2003) also found the effects of indirect processes for Fe XX-Fe XXV lines to be smaller than 10%. While these calculations provide additional support for our choice of Fe lines and add confidence to the propriety of the atomic data, demonstrable problems still remain in the case of Fe XVIII. Desai et al. (2005) found good agreement between the predicted fluxes for the Fe XVIII lines at 14.21Å and 14.26Å obtained from the CHIANTI and Flexible Atomic Code (Gu 2003b), which includes the DR processes. However, the fluxes observed in *Chandra* grating spectra of Capella are ∼50% higher than expected based on normalisation to the EUV $2s$-$2p$ transitions, with the likely culprit being the excitation rates. Such errors in the Fe XVIII atomic data might introduce some additional structure into the best-fit DEM solutions, though this will be tempered by the statistically more significant information from the H-like and He-like ions of Mg and Si. The abundances themselves are quite insensitive to small deviations in the DEM and we do not expect the possibly errors in the Fe XVIII atomic data to have a significant impact.

In order to obtain the *differential emission measure* (DEM) we have performed a Markov-Chain Monte-Carlo analysis using a Metropolis algorithm (MCMC[M]) on the set of supplied line flux ratios (Kashyap & Drake 1998). Advantages of this method include the ability to estimate uncertainties and the avoidance of unnecessary smoothing constraints. The DEM is a measure of the amount of emitting power—correlated with the amount of emitting

material—as a function of temperature in the coronal plasma. It is formally defined as:

$$\Phi(T) = n_e^2 \frac{dV(T)}{dlogT} \tag{3}$$

A given line flux depends on both temperature and on the abundance of the element in question. The ratio of two emission lines from ions of the *same* element is independent of the abundance of the chosen element. We have therefore devised a method that uses line *ratios* instead of line fluxes directly (García-Alvarez et al. 2005) (A similar method was developed independently by Schmitt & Ness (2004)). The MCMC[M] method yields the emission measure distribution over a pre-selected temperature grid, where the DEM is defined for each T bin. In our case, a set of temperatures T_n, with Δ log $T[K]$=0.1 and ranging from log T=6.2 to log $T[K]$=7.5, define the $\Phi(T_n)$. The derived $\Phi(T_n)$ is only reliable over a certain temperature range if we have enough lines with contribution function G(T_{max})$\sim$ G(T_n).

Based on the lines we use in our analysis we are able to obtain a well-constrained DEM(T_n) between log $T[K]$=6.2 (coolest peak formation temperature given by the resonance line O VII is log $T[K]$=6.3) and log $T[K]$=7.5 (hottest peak formation temperature given by the resonance line S XVI is log $T[K]$=7.4); larger uncertainties are obtained outside that range. The H-like and He-like lines constrain the structure of the DEM in the upper and lower temperature range, while the iron ions give information about the structure of the DEMs in the intermediate range. The MCMC[M] code returns the DEM, among any user-defined number of possible DEMs that are generated based on the MCMC method, that best reproduces the observed fluxes. As noted above, one product of our MCMC[M] method is the statistical uncertainties in $\Phi(T)$ evaluated at the 68% confidence level. One has to bear in mind that the error bars for consecutive bins in DEMs are not independent, owing to the inevitable cross-talk that arises as a result of the line contribution functions themselves stretching over several bins. While our DEM method imposes a degree of local smoothing, dictated by the number of diagnostic lines with significant emission in each temperature bin (see Kashyap & Drake 1998, for details), this smoothing is not always sufficient to attenuate "high frequency oscillations" in the solution—the artifact whereby overly high values of the DEM in a given temperature bin can be compensated for by a commensurately lower value in adjacent bins. In principle, there is no limit to the scale of the high-frequency oscillations. In practice, the binning inherent in the temperature grid serves as a de-factor smoothing scale that eliminates all oscillations unresolved by the grid. Our final DEMs are corrected for the distances of the stars.

4.4. Abundances

In comparing the coronal abundance results with underlying photospheric values it is tempting to adopt a photospheric mixture different to that of the Sun to accomodate small deviations from such a mixture that might have been found in the different photospheric studies. However, as discussed in §2, of our sample only the photospheric composition of β Ceti has been studied in any detail. Close examination of the results listed in Table 2 (which have been scaled relative to the abundance mixture of Asplund et al. (2004)), however, reveals very little evidence for a significant deviation from a solar mixture. Exceptions are, possibly, Si, which appears slightly over-abundant compared to Fe in the Ottmann et al. (1998) study, with an indication of a similar trend in the earlier work of McWilliam (1990) and Luck & Challener (1995). Na also appears slightly over-abundant in the studies of Kovacs (1983), Luck & Challener (1995), and Drake (unpublished). The latter might be related to the Ne-Na cycle which can enhance the Na abundance in the post-dredge-up envelopes of giants stars (e.g. Denisenkov & Ivanov 1987; Drake et al. 1994a; Langer & Hoffman 1995; Weiss et al. 2000). However, as becomes clear in the coronal abundances, there is no evidence for significantly enhanced Si, and we have only upper limits for the fluxes of the available Na lines in our spectra. We therefore adopt the mixture of Asplund et al. (2004) for comparing all coronal abundanc results. Asplund et al. (2004) revision of the solar chemical composition shows a downward by 25-35% of the abundances of light elements such as C, N, O and Ne compare with values from earlies studies (e.g. Grevesse & Sauval 1998). The use of these new values would increase the derived stellar coronal abundances of light elements relative to those obtained by using the solar chemical composition from earlies studies. In order words, the observed trends in the FIP effect and in the inverse-FIP effect will be slighlty shallower and slightly steeper respectively if one uses the new solar chemical composition reported by Asplund et al. (2004).

One exception to the Asplund et al. (2004) mixture might be the element Ne. Drake & Testa (2005) have recently found Ne/O to be enhanced by an average factor of 2.7 compared to the Asplund et al. (2004) ratio in the coronae of approximately 20 nearby stars. Based on this results, we have assumed a Ne abundance revised upward by 0.43 dex with respect to Asplund et al. (2004). In the discussion that follows, we therefore also examine the effects of a higher photospheric Ne abundance.

Once the DEM has been established, we can evaluate the abundances of any elements for which we have lines with measured fluxes. We derive values for the coronal abundances of the elements Ne, O, S, Si, Fe, Mg, Al and Na, though only upper limits were obtained for the abundances of Na and Al, owing to the lack of signal in their respective line features (see Table 5 and Table 6). If there is more than one line for an element, then the abundance

is computed as the weighted average of the abundance determinations from each of the individual lines.

We also used the temperature-insensitive abundance ratio diagnostics of Drake et al. (2005) as an additional check on our values obtained using the DEM. These are ratios formed by combining two sets of lines of two different elements, constructed such that the combined emissivity curves of each set have essentially the same temperature dependence. The resulting ratio of measured line fluxes then yields directly the ratio of the abundances of the relevant elements, independent from the atmospheric temperature structure. A similar, though less sophisticated method, has been previously used in solar coronal observations (e.g. Feldman 1992; Feldman & Laming 2000) and in stellar EUVE observations (Drake et al. 1995, 1997).

5. Results and Discussion

In order to verify the propriety of our DEM and abundance techniques we have compared observed and modeled line fluxes vs ionic species in Fig 3 (upper panel) and vs T_{max} (lower panel) for β Cet, 31 Com and μ Vel (ID1890 and ID3410) and for the final DEMs and abundances. All the predicted line fluxes based on our final models are within 10 % or so of the observed values.

Fig 7 shows the observed and synthetic spectra of β Cet, 31 Com and μ Vel. For these spectra, we have used an electron density of $n_e = 1.8\,10^{12} cm^{-3}$ for β Cet, $n_e = 3.2\,10^{12} cm^{-3}$ for 31 Com and $n_e = 1.0\,10^{12} cm^{-3}$ for μ Vel derived by Testa et al. (2004), and an interstellar medium column density of $n_H = 1\,10^{18} cm^{-2}$. Although the n_H for μ Vel could be underestimated the exact value for the ISM column makes no practical difference to the synthetic spectra below 50 Å. All the synthetic spectra showing good qualitative agreement with observations for the three stars.

5.1. Temperature Structure

Fig. 4 shows the reconstructed DEMs for β Cet, 31 Com and μ Vel. The DEMs for β Cet and μ Vel are all quite similar in overall shape and normalisation although the former is 2-3 times brighter. Both exhibit a broad peak around $\log T[\mathrm{K}] \sim 6.8 \pm 0.2$, while 31 Com shows a smooth increase reaching a peak at $\log T[\mathrm{K}] \sim 7.1$. The DEMs for the three stars show little evidence for substantial amount of plasma at temperatures higher than $\log T[\mathrm{K}] = 7.3$. Nevertheless, 31 Com seems to have more plasma at higher temperatures compared with β

Cet and μ Vel. It also has a higher X-ray luminosity (see Table 1).

We note the similarity in β Cet, 31 Com and μ Vel thermal structures in the low temperature range (log T[K]=6.4-6.7). For μ Vel and β Cet we find a perfect match even for lower temperatures and for higher temperatures up to log T[K]=7.2. The slopes in the derived DEMs on the low temperature side of their maxima follow very approximately the relation DEM$\propto$T^5 for β Cet and μ Vel and DEM$\propto$T$^{5/2}$ for 31 Com, which is steeper than the DEM$\propto$T$^{3/2}$ suggested for quasi-static coronal loops (e.g.; Craig et al. 1978; Jordan 1980; Peres et al. 2000).

Our results for 31 Com are comparable with those reported by Ayres et al. (1998) and Scelsi et al. (2004) based on *EUVE* and XMM-*Newton* observations respectively. Scelsi et al. (2004) obtained a single-peak DEM with a sharper increase for the lower temperatures, log T[K]<6.8, and smooth decrease for the higher temperatures, log T[K]>7.2. The Scelsi et al. (2004) line-based DEM also shows a maximum at log T[K]$\sim$7.0$\pm$0.1. Ayres et al. (1998) also derived, based on *EUVE* observations, the DEM for β Cet. They obtained a thermal structure that peaks at log T[K]$\sim$6.8 showing a smooth decrease thereafter. To our knowledge, there exist no other DEM analysis of μ Vel by other authors with which to compare our temperature structure results.

5.2. Coronal Abundances

Our results for the element abundances of β Cet, 31 Com and μ Vel are summarized in Table 5. We only list statistical uncertainties here. The formal error estimate for the abundances reflects only the uncertainty of the observed fluxes together with the uncertainty in the estimated DEM. This is done by examining the distribution of synthetic fluxes around the best fit flux, as computed from the collection of DEMs sampled by the MCMC method. There are of course other uncertainties in the atomic data used for the analysis, and in the calibration of the *Chandra* instruments. Atomic data uncertainties are probably of order 30% for Fe lines (e.g.; Drake et al. 1995), but are probably slightly less than this for H-like and He-like lines. These uncertainties are, however, systematic in nature and will partially cancel when lines of different ionization stages and multiplets are used to estimate abundances. Uncertainties in instrument calibration are of order 10% and will also be systematic in nature. The final uncertainties in our derived abundances are difficult to assess rigorously, but are likely of order 0.1 dex.

The abundance ratios derived from temperature-insensitive line ratios are listed in Table 6. These values are in agreement with, and provide verification for, the ones derived

from the DEMs (Table 5), with the exception of the ratios involving Fe. As noted by Drake et al. (2005), however, these ratios are likely to exhibit larger systematic errors owing to a less optimum coincidence of the different line contribution functions as a function of temperature.

In Fig. 5 we have plotted the derived abundances, relative to the adopted stellar photospheric values (essentially the mixture of Asplund et al. (2004), with the exception of Ne for which we adopt the Drake et al. (2005) value, as discussed earlier), in order of element FIP, for β Cet, 31 Com and μ Vel. Despite almost an order of magnitude range in rotational velocity among this small sample of late-type giants they clearly share similarities in coronal composition. Our analysis shows a slight change in the trend of the coronal abundance vs FIP from the less evolved 31 Com (very little or no trend with FIP) to the more evolved β Cet and μ Vel (some trend with FIP discernible). β Cet and μ Vel show the same general abundance pattern, characterised by a depletion of high FIP elements (O, Ne) by a factor of ~ 2, and with no evidence for significant depletions of the low FIP elements (Mg, Fe and Si) relative to stellar photospheric abundances.

The FIP effect observed for β Cet and μ Vel is similar to those seen in other low to intermediate activity stars (Drake et al. 1994b, 1995, 1997; Güdel et al. 2002). We emphasise that there is some uncertainty in the absolute normalisation of the derived abundances compared with assessed photospheric values, such that we cannot determine with certainty whether or not the low FIP elements in β Cet and μ Vel are truly photospheric and the high FIP elements depleted, or whether the high FIP elements are photospheric and the low FIP elements are enhanced. We also note that there is no definitive information regarding the exact photospheric abundances of the elements in question, and observed coronal abundance trends should be treated with some caution. Nevertheless, the similarity of the abundance results for β Cet and μ Vel and the general FIP effect trends seen for other stars compared with the well-established solar photospheric baseline does lend some support to the coronal abundance anomaly interpretation.

We also add slight caution in interpreting the absolute Ne abundance. It can be seen from comparison of the Ne/O ratios obtained from DEM modelling and temperature-insensitive line diagnostics (Table 6) that the former method tends to arrive at a slightly lower Ne abundance than the latter. Uncertainties in both methods are of order 0.1 dex (see also Drake et al. 2005), so the current discrepency is not beyond the bounds of the systematic errors of the two approaches. The Drake et al. (2005) study suggests Ne is enhanced with respect to O by a factor of 2.7 as compared to Asplund et al. (2004): while the temperature-insensitive ratios are in general agreement with this, our DEM results indicate a number somewhat lower, and closer to a factor of 1.7 or so. Adopting a lower value for the photospheric Ne abundance would raise the Ne points in Figure 5 (and in Fig. 6 described

below). While it is not possible to state definitively which Ne/O abundance ratio is the more accurate, it is possible that the DEM method might slightly overestimate the O abundance relative to that of Ne by virtue of the DEM being restricted to temperatures $\log T > 6.3$: omission of the cooler material can be compensated for in the analysis of line fluxes by an increased abundance. In the case of O, whose Ne-like and H-like lines are formed at cooler temperatures in general than those of Ne, this might plausibly lead to a slightly lower Ne/O ratio.

In Fig. 6 we plot the abundance results from earlier studies of β Cet and 31 Com (Drake et al. 1994b; Maggio et al. 1998; Scelsi et al. 2004). It is important to note that different authors adopt different values for "solar" photospheric abundances: for the Fig. 6 we have scaled the various abundance results to the Asplund et al. (2004) mixture. Despite the fact that the coronal abundances for β Cet were derived from low resolution spectra there is reasonable agreement with our results in the general trend observed as a function of FIP for both β Cet and 31 Com.

Despite Mg, Fe and Si having very similar FIP, there is a hint in our results for a small depletion of Fe relative to Mg and Si by ~ 0.1 dex. This has also been seen in other coronal abundance studies, as summarised by Drake (2003) who suggested gravitational settling of the heavier Fe ions as a possible explanation. However, the low surface gravity of these giants argues against such a mechanism—gravitational settling should be negligible in these stars. Instead, a more likely explanation is systematic error.

It is tempting to interpret the small differences in coronal abundance between 31 Com and the more evolved giants in terms of trends with stellar activity. As first suggested by schematically by Drake et al. (1995) and later fleshed out by Audard et al. (2003) for active binaries and Telleschi et al. (e.g. 2005) for dwarfs, the FIP effect characterising lower activity stars, including the Sun, is seen to change to an inverse-FIP effect in more active stars. Although the trends observed in our work change in a similar manner, relative to the rotation of these stars, we speculate instead that the differences can be attributed primarily to their different evolutionary status and consequent differences in the properties of their envelopes that are likely the site of underlying dynamo activity.

These giant stars have A and late B progenitors on the main sequence which have no outer convection zones. As a late-type giant evolves from the Herztsprung gap (31 Com) to the "clump" (β Cet), the developing convection zone deepens and magnetic braking sets in (e.g. Gray 1989). Such structural changes might well be expected to affect dynamo processes and coronal activity. Indeed, Pizzolato et al. (2000) reported that intermediate-mass stars with 0.5<B-V<0.8 (31 Com) follow $L_x \sim (v \sin i)^2$ (Pallavicini et al. 1981) while stars redder than B-V=0.8 (β Cet and μ Vel) rest well above that law. In other words, these two groups

of stars show almost the same X-ray luminosity despite a decrease in rotational velocity of almost two orders of magnitude. The maintenance of X-ray luminosity is naturally attributed to the deepening of the convective zone and possibly to an increase in differential rotation triggered by magnetic braking.

It is also interesting that large flares have been observed on both β Cet and μ Vel, yet 31 Com appears to have remained steady (Ayres et al. 2003, and earlier work referenced therein). Similar differences in gap-clump long-term variability was inferred by Johnson et al. (2002) based on HST STIS observations of Fe XXI in Capella: the clump component appears to have varied considerably compared with earlier observations, yet the gap component was observed at the same flux level.

While there are good reasons based on stellar structural arguments to expect differences in the coronae of gap and clump giants, the actual mechanisms responsible for the different abundances and temperature structures remain highly speculative for now. A recent model based on ponderomotive forces resulting from Alfvén waves (Laming 2004) is interesting in this regard. According to this model, the FIP effect results from a resonance between the chromospheric Alfvén wave spectrum engendered by turbulence in the convection zone and coronal loop length that enables the wave ponderomotive force to either suppress or enhance the movement of ions into the corona. The FIP effect or its absence therefore depends on the tuning between the coronal magnetic field and the Alfvén wave spectrum. As we have mentioned above, the Hertzsprung gap star 31 Com should have a shallower convection zone and perhaps a different differential rotation profile with depth compared with β Cet and μ Vel, which are more evolved. One might then expect different tuning between coronal structures and the ambient Alfvén wave spectrum. Qualitatively, this could give rise to the observed abundance differences. Detailed calculations of the Alfvén wave spectrum for realistic coronal structures on yellow-red giants will be needed to confirm or disprove such a model.

6. Conclusions

β Cet, 31 Com and μ Vel represent the important stages through which intermediate mass late-type giants evolve during their lifetime (the Hetzsprung gap (31 Com), the rapid braking zone (μ Vel) and the core helium burning "clump" phase (β Cet)). As such, a comparison of their coronal properties provides an illuminating glimpse of any fundamental underlying differences in their magnetic dynamos and activity. Based on an analysis of high resolution *Chandra* X-ray spectra of these stars we draw the following conclusions.

1. β Cet and μ Vel show coronal temperature structures and element abundances that are remarkably similar. Element abundances are characterized by a mild FIP-type effect in which the abundances of low FIP elements are enhanced relative to those of high FIP elements by a factor of ~ 2. While we cannot rule out this result as being a fluke of underlying photospheric, rather than coronal, abundances, the latter scenario is supported by similarities with abundance anomalies seen in low-intermediate activity dwarfs.

2. The coronal temperature structure of 31 Com differs from those of β Cet and μ Vel and exhibits a sharper peak at higher temperatures, as seen earlier by Ayres et al. (1998) based on EUVE spectra. Its corona is significantly hotter, as is evident from comparison of its spectrum with those of β Cet and μ Vel: lines formed at hotter temperatures are stronger in 31 Com, and it also has a stronger short wavelength continuum. Element abundances are characterized by a lack of an obvious FIP effect and appear closer to photospheric estimates.

3. We speculate that structural changes during the evolution of late-type giants are likely responsible for the small observed differences in coronal abundances and temperature structure. In particular, the size of the convection zone coupled with the rotation rate seem obvious choices for playing a key role in determining coronal characteristics.

DGA and WB were supported by *Chandra* grants GO1-2006X and GO1-2012X. LL was supported by NASA AISRP contract NAG5-9322; we thank this program for providing financial assistance for the development of the PINTofALE package. We also thank the CHIANTI project for making publicly available the results of their substantial effort in assembling atomic data useful for coronal plasma analysis. JJD and VK were supported by NASA contract NAS8-39073 to the *Chandra*.

REFERENCES

Alschuler, W. R. 1975, ApJ, 195, 649

Asplund, M., Grevesse, N. & Sauval, A. J. 2004, ArXiv ASprophysics e-prints, astro-ph/0410214

Audard, M., Güdel, M., Sres, A., Raassen, A. J. J., & Mewe, R. 2003, A&A, 398, 1137

Ayres, T. R., Brown, A., Drake, S., Simon, T., Stern, R. A., & Wood, B. E. 1994, Bulletin of the American Astronomical Society, 26, 1381

Ayres, T. R., Brown, A., Harper, G. M., Osten, R. A., Linsky, J. L., Wood, B. E., & Redfield, S. 2003, ApJ, 583, 963

Ayres, T. R., Brown, A., Osten, R. A., Huenemoerder, D. P., Drake, J. J., Brickhouse, N. S., & Linsky, J. L. 2001, ApJ, 549, 554

Ayres, T. R., et al. 1995, ApJS, 96, 223

Ayres, T. R., Osten, R. A., & Brown, A. 1999, ApJ, 526, 445

Ayres, T. R., Schiffer, F. H., & Linsky, J. L. 1983, ApJ, 272, 223

Ayres, T. R., Simon, T., Stern, R. A., Drake, S. A., Wood, B. E., & Brown, A. 1998, ApJ, 496, 428

Brown, J. A., Sneden, C., Lambert, D. L., & Dutchover, E. J. 1989, ApJS, 71, 293

Burnashev, V. I. 1983, Izvestiya Ordena Trudovogo Krasnogo Znameni Krymskoj Astrofizicheskoj Observatorii, 67, 13

Craig, I. J. D., McClymont, A. N., & Underwood, J. H. 1978, A&A, 70, 1

de Medeiros, J. R. & Mayor, M. 1995, A&A, 302, 745

Denisenkov, P. A. and Ivanov, V. V. 1987, Pis ma Astronomicheskii Zhurnal , 13, 520

Dere, K. P., Landi, E., Young, P. R., & Del Zanna, G. 2001, ApJS, 134, 331

Desai, P., et al. 2005, ApJ, 625, L59

Doron, R. & Behar, E. 2002, ApJ, 574, 518

Drake, J. 2004, Chandra News, 11, 8

Drake, J. J. 2003, Advances in Space Research, 32, 945

Drake, J. J., Laming, J. M., Lin, L., & Kashyap, V. 2005, ApJ

Drake, J. J., Laming, J. M., & Widing, K. G. 1995, ApJ, 443, 393

—. 1997, ApJ, 478, 403

Drake, J. J. & Testa, P. 2005, Nature, 436, 525

Drake, S. A., Singh, K. P., White, N. E., & Simon, T. 1994a, ApJ, 436, L87

—. 1994b, ApJ, 436, L87

Favata, F., Barbera, M., Micela, G., & Sciortino, S. 1995, A&A, 295, 147

Favata, F., Reale, F., Micela, G., Sciortino, S., Maggio, A., & Matsumoto, H. 2000, A&A, 353, 987

Favata, F. & Schmitt, J. H. M. M. 1999, A&A, 350, 900

Feldman, U. 1992, Physica Scripta Volume T, 46, 202

Feldman, U. & Laming, J. M. 2000, Phys. Scr, 61, 222

Foing, B. H., et al. 1994, A&A, 292, 543

Güdel, M., Audard, M., Briggs, K., Haberl, F., Magee, H., Maggio, A., Mewe, R., Pallavicini, R., & Pye, J. 2001, A&A, 365, L336

Güdel, M., Audard, M., Sres, A., Wehrli, R., Behar, E., Mewe, R., Raassen, A. J. J., & Magee, H. R. M. 2002, in ASP Conf. Ser. 277: Stellar Coronae in the Chandra and XMM-NEWTON Era, 497

García-Alvarez, D., Drake, J. J., Lin, L., Kashyap, V., & Ball, W. N. 2005, 621, 1009, ApJ

García-Alvarez, D., et al. 2003, A&A, 397, 285

Gondoin, P. 1999, A&A, 352, 217

Gratton, R. G. & Ortolani, S. 1986, A&A, 169, 201

Gray, D. F. 1989, ApJ, 347, 1021

Grevesse, N. & Sauval, A. J. 1998, Space Science Reviews, 85, 161

Gu, M. F. 2003, ApJ, 593, 1249

—. 2003b, ApJ, 582, 1241

Gustafsson, B., Kjaergaard, P., & Andersen, S. 1974, A&A, 34, 99

Holweger, H. 1979, 22nd Liege Int.Astr.Symp., p117

Johnson, O., Drake, J. J., Kashyap, V., Brickhouse, N. S., Dupree, A. K., Freeman, P., Young, P. R., & Kriss, G. A. 2002, ApJ, 565, L97

Jones, K. L., Robinson, R. D., Slee, O. B., & Stewart, R. T. 1992, MNRAS, 256, 535

Jordan, C. 1980, A&A, 86, 355

Kashyap, V. & Drake, J. J. 1998, ApJ, 503, 450

—. 2000, Bulletin of the Astronomical Society of India, 28, 475

Kovacs, N. 1983, A&A, 120, 21

Lambert, D. L. & Ries, L. M. 1981, ApJ, 248, 228

Laming, J. 2004, ApJ

Langer, G. E. & Hoffman, R. D. 1995, PASP, 107, 1177

Luck, R. E. & Challener, S. L. 1995, AJ, 110, 2968

Maggio, A., Favata, F., Peres, G., & Sciortino, S. 1998, A&A, 330, 139

Maggio, A., Pallavicini, R., Reale, F., & Tagliaferri, G. 2000, A&A, 356, 627

Maggio, A., Vaiana, G. S., Haisch, B. M., Stern, R. A., Bookbinder, J., Harnden, F. R., & Rosner, R. 1990, ApJ, 348, 253

Makarov, V. V. 2003, AJ, 126, 1996

Mallik, S. V., Parthasarathy, M., & Pati, A. K. 2003, A&A, 409, 251

Mazzotta, P., Mazzitelli, G., Colafrancesco, S., & Vittorio, N. 1998, A&AS, 133, 403

McWilliam, A. 1990, ApJS, 74, 1075

Mewe, R., Kaastra, J. S., van den Oord, G. H. J., Vink, J., & Tawara, Y. 1997, A&A, 320, 147

Ness, J., Brickhouse, N. S., Drake, J. J., & Huenemoerder, D. P. 2003, ApJ, 598, 1277

Ortolani, A., Pallavicini, R., Maggio, A., Reale, F., & White, S. M. 1998, in ASP Conf. Ser. 154: Cool Stars, Stellar Systems, and the Sun, 1532

Ottmann, R., Pfeiffer, M. J., & Gehren, T. 1998, A&A, 338, 661

Ottmann, R. & Schmitt, J. H. M. M. 1996, A&A, 307, 813

Pallavicini, R., Golub, L., Rosner, R., Vaiana, G. S., Ayres, T., & Linsky, J. L. 1981, ApJ, 248, 279

Parker, E. N. 1970, ARA&A, 8, 1

Peres, G., Orlando, S., Reale, F., Rosner, R., & Hudson, H. 2000, ApJ, 528, 537

Perryman, M. A. C., et al. 1997, A&A, 323, L49

Pizzolato, N., Maggio, A., & Sciortino, S. 2000, A&A, 361, 614

Raassen, A. J. J., Mewe, R., Audard, M., Güdel, M., Behar, E., Kaastra, J. S., van der Meer, R. L. J., Foley, C. R., & Ness, J.-U. 2002, A&A, 389, 228

Sanz-Forcada, J., Favata, F., & Micela, G. 2004, A&A, 416, 281

Scelsi, L., Maggio, A., Peres, G., & Gondoin, P. 2004, A&A, 413, 643

Schaller, G., Schaerer, D., Meynet, G., & Maeder, A. 1992, A&AS, 96, 269

Schmitt, J. H. M. M. & Ness, J.-U. 2002, A&A, 388, 13

Schmitt, J. H. M. M. & Ness, J.-U. 2004, A&A, 415, 1099

See, T. J. J. 1897, AJ, 17, 119

Siess, L. & Livio, M. 1999, MNRAS, 308, 1133

Simon, T. 1984, ApJ, 279, 738

Simon, T. & Drake, S. A. 1989, ApJ, 346, 303

Smith, M. A. & Dominy, J. F. 1979, ApJ, 231, 477

Strassmeier, K. G., Washuttl, A., & Rice, J. B. 1994, Informational Bulletin on Variable Stars, 3994, 1

Taylor, B. J. 1999, A&AS, 134, 523

Telleschi, A., Güdel, M., Briggs, K., Audard, M., Ness, J., & Skinner, S. L. 2005, ApJ, 622, 653

Testa, P., Drake, J. J., & Peres, G. 2004, ApJ

Ueda, Y., Ishisaki, Y., Takahashi, T., Makishima, K., & Ohashi, T. 2001, ApJS, 133, 1

Weiss, A., Denissenkov, P. A., & Charbonnel, C. 2000, A&A, 356, 181

White, N. E., Arnaud, K., Day, C. S. R., Ebisawa, K., Gotthelf, E. V., Mukai, K., Soong, Y., Yaqoob, T., & Antunes, A. 1994, PASJ, 46, L97

Wilson, O. C. 1966, ApJ, 144, 695

Tables

Table 1. Summary of Stellar Parameters.

Star	HD	Sp. Type	B-V	D [pc]	$R_\odot$	$M_\odot$	$g_\odot$	T_{eff} [K]	$v \sin i$ [km s^{-1}]	log L_x [erg s^{-1}]
31 Com	111812	G0 III[e]	0.67[e]	94[b]	9.3[e]	2.9[e]	0.039	5320[h]	66.5[f]	30.9[d]
μ Vel	93497	G5 III[a]	0.91[a]	36[b]	13.0[g]	3.0[g]	0.016	4862[i]	6.4[f]	30.3[d]
β Cet	4128	G9.5 III[a]	1.02[a]	29[b]	15.1[c]	3.0[c]	0.022	4840[h]	3.0[c]	30.4[d]

[a]Makarov (2003)

[b]Perryman et al. (1997)

[c]Ayres et al. (1998)

[d]Derived from our *Chandra* observations (0.5-2.4 KeV).

[e]Pizzolato et al. (2000)

[f]de Medeiros & Mayor (1995)

[g]Ayres et al. (1999)

[h]Gondoin (1999)

[i]Favata et al. (1995)

Table 2: β Cet, 31 Com, μ Vel photospheric abundances[a] from literature and adopted here.

β Cet											
T_{eff}	log g	ξ	[Na/H]	[Al/H]	[Mg/H]	[Fe/H]	[Si/H]	[S/H]	[O/H]	[Ne/H]	References
4 810	2.34	1.5	···	···	···	0.00±0.15	···	···	+0.02±0.16	···	Lambert & Rie
4 800	2.50	2.3	+0.63±0.24	+0.23	+0.01±0.28	-0.10±0.16	+0.04±0.27	···	···	···	Kovacs (1983)
4 840	2.80	···	···	···	···	+0.16	···	···	···	···	Burnashev (198
4 860	2.80	1.6	···	···	···	+0.09±0.08	···	···	+0.15±0.19	···	Gratton & Ort
4 800	2.40	1.7	···	···	···	+0.26	···	···	···	···	Brown et al. (1
4 820	2.87	2.2	···	···	···	+0.13±0.11	0.22	···	···	···	McWilliam (19
5 000	2.75	1.7	···	···	···	+0.37±0.12	···	···	···	···	Jones et al. (19
4 750	2.65	2.4	+0.52±0.12	+0.23	···	+0.20±0.27	+0.42±0.18	···	···	···	Luck & Challe
4 800	2.80	1.6	···	···	+0.02±0.05	+0.12±0.05	+0.31±0.05	···	···	···	Ottmann et al.
4 850	2.40	1.6	+0.48±0.2	···	···	+0.24±0.2	···	···	···	···	J. Drake[c]
31 Com											
T_{eff}	log g	ξ	[Na/H]	[Al/H]	[Mg/H]	[Fe/H]	[Si/H]	[S/H]	[O/H]	[Ne/H]	References
5 550	3.00	1.7	···	···	···	-0.05±0.10	···	···	···	···	Gustafsson et a
5 680	3.00	1.7	···	···	···	-0.11±0.10	···	···	···	···	Taylor (1999)
μ Vel											
T_{eff}	log g	ξ	[Na/H]	[Al/H]	[Mg/H]	[Fe/H]	[Si/H]	[S/H]	[O/H]	[Ne/H]	References
5 180	2.60	···	···	···	···	-0.07	···	···	···	···	Burnashev (198

[a]Note that all the photospheric abundances are scaled to the values given by Asplund et al. (2004)

[b]We list here the formal "internal" accuracy stated by Ottmann et al. (1998). As these authors indicate, the true uncertainties will be significantly higher owing to systematic uncertainties.

[c]J. Drake unpublished, based on spectra obtained at McDonald Observatory 82" telescope and echelle spectrograph.

Table 3. Summary of *Chandra* HETG+ACIS-S Observations.

Star	ObsID	Start [UT]	Exp [ks]
31 Com	1891	2001-03-12T15:03:38	130.2
μ Vel	3410	2001-12-18T19:23:14	57.0
μ Vel	1890	2001-09-24T08:35:16	19.7
β Cet	974	2001-06-29T23:29:11	86.1

Table 4: Identification and fluxes for spectral lines, observed on β Cet, 31 Com, μ Vel (ObsID 3410 and ObsID 1890), used in this analysis.

λ_{obs} [Å]	λ_{pred} [Å]	Ion	$log\,T_{max}$ [K]	31 Com [10^{14} erg cm^{-2} s^{-1}]	μ Vel (ObsID 3410) [10^{14} erg cm^{-2} s^{-1}]	μ Vel (ObsID 1890) [10^{14} erg cm^{-2} s^{-1}]	β Cet [10^{14} erg cm^{-2} s^{-1}]	Transition (upper $\rightarrow$ lower)
4.722	4.727	S XVI	7.40	0.32 ± 0.35	0.45 ± 0.42	···	1.85 ± 1.09	$(2p)\ ^2P_{3/2} \rightarrow (1s)\ ^2S_{1/2}$
···	4.733	S XVI	7.40	0.16 ± 0.17	0.23 ± 0.21	···	0.93 ± 0.54	$(2p)\ ^2P_{1/2} \rightarrow (1s)\ ^2S_{1/2}$
5.032	5.039	S XV	7.20	1.83 ± 0.69	1.35 ± 1.22	···	8.37 ± 1.51	$(1s2p)\ ^1P_1 \rightarrow (1s^2)\ ^1S_0$
6.177	6.180	Si XIV	7.20	3.77 ± 0.33	3.15 ± 0.52	1.04 ± 1.13	8.28 ± 0.59	$(2p)\ ^2P_{3/2} \rightarrow (1s)\ ^2S_{1/2}$
···	6.186	Si XIV	7.20	1.88 ± 0.16	1.57 ± 0.26	0.52 ± 0.57	4.14 ± 0.29	$(2p)\ ^2P_{1/2} \rightarrow (1s)\ ^2S_{1/2}$
6.647	6.648	Si XIII	7.00	5.70 ± 0.44	9.42 ± 0.83	9.04 ± 1.56	20.74 ± 0.96	$(1s2p)\ ^1P_1 \rightarrow (1s^2)\ ^1S_0$
7.176	7.176	Al XIII	7.10	0.14 ± 0.04	0.21 ± 0.21	···	0.18 ± 0.09	$(2p)\ ^2P_{1/2} \rightarrow (1s)\ ^2S_{1/2}$
···	7.171	Al XIII	7.10	0.27 ± 0.09	0.43 ± 0.43	···	0.36 ± 0.18	$(2p)\ ^2P_{3/2} \rightarrow (1s)\ ^2S_{1/2}$
7.732	7.757	Al XII	6.90	0.82 ± 0.30	1.64 ± 0.51	···	2.06 ± 0.49	$(1s2p)\ ^1P_1 \rightarrow (1s^2)\ ^1S_0$
8.422	8.425	Mg XII	7.00	1.64 ± 0.15	2.85 ± 0.29	2.37 ± 0.57	7.85 ± 0.28	$(2p)\ ^2P_{1/2} \rightarrow (1s)\ ^2S_{1/2}$
···	8.419	Mg XII	7.00	3.28 ± 0.30	5.70 ± 0.58	4.75 ± 1.14	15.72 ± 0.56	$(2p)\ ^2P_{3/2} \rightarrow (1s)\ ^2S_{1/2}$
9.173	9.169	Mg XI	6.80	2.30 ± 0.29	10.06 ± 0.79	9.37 ± 1.43	22.30 ± 0.93	$(1s2p)\ ^1P_1 \rightarrow (1s^2)\ ^1S_0$
10.028	10.029	Na XI	6.90	0.29 ± 0.10	1.26 ± 0.30	1.67 ± 0.87	2.08 ± 0.24	$(2p)\ ^2P_{1/2} \rightarrow (1s)\ ^2S_{1/2}$
···	10.023	Na XI	6.90	0.57 ± 0.19	2.52 ± 0.60	3.33 ± 1.74	4.16 ± 0.48	$(2p)\ ^2P_{3/2} \rightarrow (1s)\ ^2S_{1/2}$
10.998	11.003	Na X	6.70	2.33 ± 0.36	2.77 ± 0.95	1.49 ± 1.38	7.94 ± 0.90	$(1s2p)\ ^1P_1 \rightarrow (1s^2)\ ^1S_0$
12.133	12.132	Ne X	6.80	6.24 ± 0.46	13.37 ± 0.88	11.51 ± 1.55	37.49 ± 1.12	$(2p)\ ^2P_{3/2} \rightarrow (1s)\ ^2S_{1/2}$
···	12.137	Ne X	6.80	3.12 ± 0.23	6.68 ± 0.44	5.75 ± 0.77	18.73 ± 0.56	$(2p)\ ^2P_{1/2} \rightarrow (1s)\ ^2S_{1/2}$
12.283	12.285	Fe XXI	7.00	7.70 ± 0.64	9.71 ± 1.03	5.25 ± 1.56	24.98 ± 1.25	$(2s^2 2p^3 d)\ ^3D_1 \rightarrow (2s^2 2p^2)\ ^3P_0$
13.433	13.447	Ne IX	6.60	1.75 ± 0.53	9.49 ± 1.43	9.56 ± 2.94	20.07 ± 1.63	$(1s2p)\ ^1P_1 \rightarrow (1s^2)\ ^1S_0$
13.508	13.504	Fe XIX	6.90	3.76 ± 0.41	9.06 ± 0.99	7.69 ± 2.02	23.14 ± 1.16	$(2p^3(^2P)3d)\ ^1D_2 \rightarrow (2s^2 2p^4)\ ^3P_2$
14.208	14.208	Fe XVIII	6.90	1.82 ± 0.29	8.99 ± 0.85	6.83 ± 1.48	20.66 ± 0.94	$(2p^4(^1D)3d)\ ^2P_{3/2} \rightarrow (2s^2 2p^5)\ ^2P_{3/2}$
···	14.203	Fe XVIII	6.90	3.43 ± 0.56	17.01 ± 1.61	12.91 ± 2.80	39.07 ± 1.78	$(2p^4(^1D)3d)\ ^2D_{5/2} \rightarrow (2s^2 2p^5)\ ^2P_{3/2}$
14.263	14.267	Fe XVIII	6.90	0.65 ± 0.23	3.26 ± 0.88	3.73 ± 2.44	7.60 ± 1.09	$(2p^4(^1D)3d)\ ^2F_{5/2} \rightarrow (2s^2 2p^5)\ ^2P_{3/2}$
15.013	15.015	Fe XVII	6.75	8.32 ± 1.12	63.06 ± 4.21	63.37 ± 7.70	129.30 ± 3.60	$(2p^5 3d)\ ^1P_1 \rightarrow (2p^6)\ ^1S_0$
16.008	16.007	O VIII	6.50	1.59 ± 0.24	3.89 ± 0.50	3.08 ± 0.78	9.19 ± 0.56	$(3p)\ ^2P_{1/2} \rightarrow (1s)\ ^2S_{1/2}$
···	16.006	O VIII	6.50	3.17 ± 0.47	7.75 ± 1.00	6.14 ± 1.55	18.31 ± 1.12	$(3p)\ ^2P_{3/2} \rightarrow (1s)\ ^2S_{1/2}$
18.973	18.973	O VIII	6.50	4.90 ± 0.63	13.67 ± 1.60	12.72 ± 3.13	30.38 ± 1.56	$(2p)\ ^2P_{1/2} \rightarrow (1s)\ ^2S_{1/2}$
···	18.967	O VIII	6.50	9.80 ± 1.27	27.37 ± 3.20	25.45 ± 6.26	60.80 ± 3.12	$(2p)\ ^2P_{3/2} \rightarrow (1s)\ ^2S_{1/2}$
21.607	21.602	O VII	6.30	3.12 ± 1.83	6.04 ± 4.60	4.00 ± 8.89	7.72 ± 2.69	$(1s2p)\ ^1P_1 \rightarrow (1s^2)\ ^1S_0$
24.777	24.779	N VII	6.30	···	7.05 ± 2.73	···	62.99 ± 5.1	$(2p)\ ^2P_{3/2} \rightarrow (1s)\ ^2S_{1/2}$
···	24.785	N VII	6.30	···	3.52 ± 1.36	···	31.48 ± 2.6	$(2p)\ ^2P_{1/2} \rightarrow (1s)\ ^2S_{1/2}$

Table 5: Coronal abundances obtained from abundance-independent DEM-reconstructions.

Element[a]	FIP[b]	31 Com	μ Vel (ObsID 3410)	μ Vel (ObsID 1890)	β Cet
Na/H	5.14	<+0.79[c]	<+1.04[c]	<+0.81[c]	<+0.93[c]
Al/H	5.98	<-0.02[c]	<+0.20[c]	···	<+0.08[c]
Mg/H	7.65	-0.12± 0.04	+0.08± 0.03	+0.11± 0.08	-0.01± 0.02
Fe/H	7.87	-0.21± 0.04	-0.03± 0.03	-0.06± 0.07	-0.12± 0.01
Si/H	8.15	-0.02± 0.03	+0.09± 0.04	+0.05± 0.11	-0.05± 0.02
S/H	10.36	-0.20± 0.16	-0.15± 0.31	···	+0.06± 0.08
O/H	13.62	-0.11± 0.08	-0.18± 0.07	-0.27± 0.16	-0.20± 0.03
Ne/H	21.56	-0.37± 0.04	-0.41± 0.04	-0.45± 0.08	-0.40± 0.02

[a]Logarithmic abundances relative to the abundance mixture of Asplund et al. (2004) with Ne from Drake & Testa (2005) (see Table 2 and discussion in §5.2).
[b]First Ionization Potential in eV.
[c]Upper limits due to lack of signal in line features.

Table 6: β Cet, 31 Com, μ Vel Abundance Ratios using Temperature-Insensitive Diagnostics.

Abundance Ratio	31 Com	31 Com[a]	μ Vel (ObsID 3410)	μ Vel[a] (ObsID 3410)	μ Vel (ObsID 1890)	μ Vel[a] (ObsID 1890)
N/O	···	···	+0.68±0.19	···	···	···
O/Ne	+0.22± 0.21	+0.26±0.12	+0.07±0.13	+0.23±0.11	+0.05±0.18	+0.18±0.24
Ne/Mg	-0.25± 0.06	-0.25±0.08	-0.50±0.04	-0.49±0.07	-0.53±0.08	-0.56±0.16
Ne/Fe	+0.17± 0.07	-0.16±0.08	-0.34±0.04	-0.38±0.07	-0.40±0.08	-0.39±0.15
Mg/Si	-0.15± 0.05	-0.10±0.07	-0.04±0.05	-0.01±0.07	-0.07±0.11	+0.06±0.19
Mg/Fe	-0.13± 0.07	+0.09±0.08	+0.06±0.05	+0.11±0.06	+0.15±0.13	+0.17±0.15
Si/S	+0.18± 0.16	+0.18±0.19	+0.27±0.34	+0.24±0.35	···	···

[a]Abundance ratios using from the DEM-reconstructions.

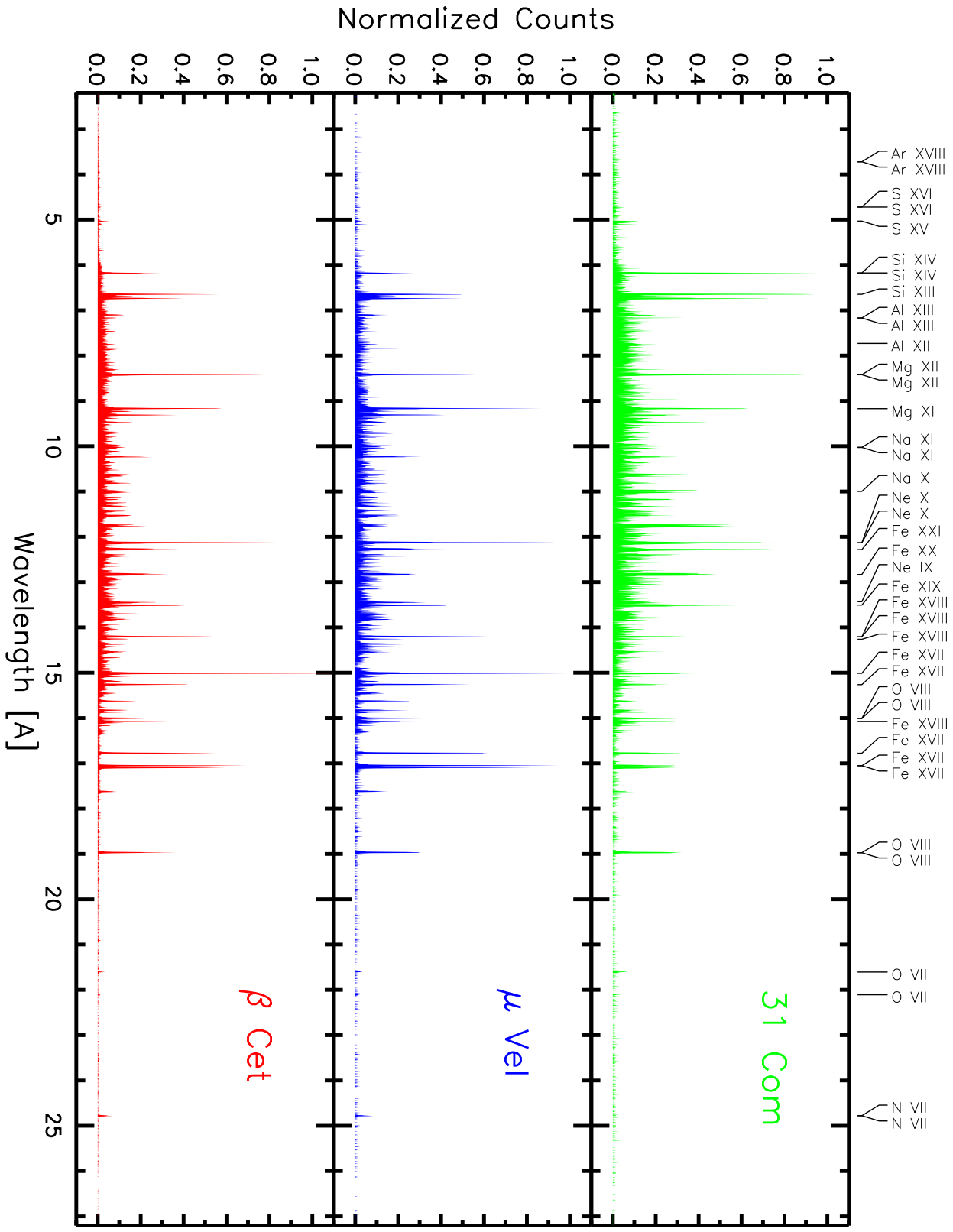

Fig. 1.— *Chandra* X-ray spectra of β Cet, 31 Com, μ Vel. The strongest lines over the observed wavelength range are identified.

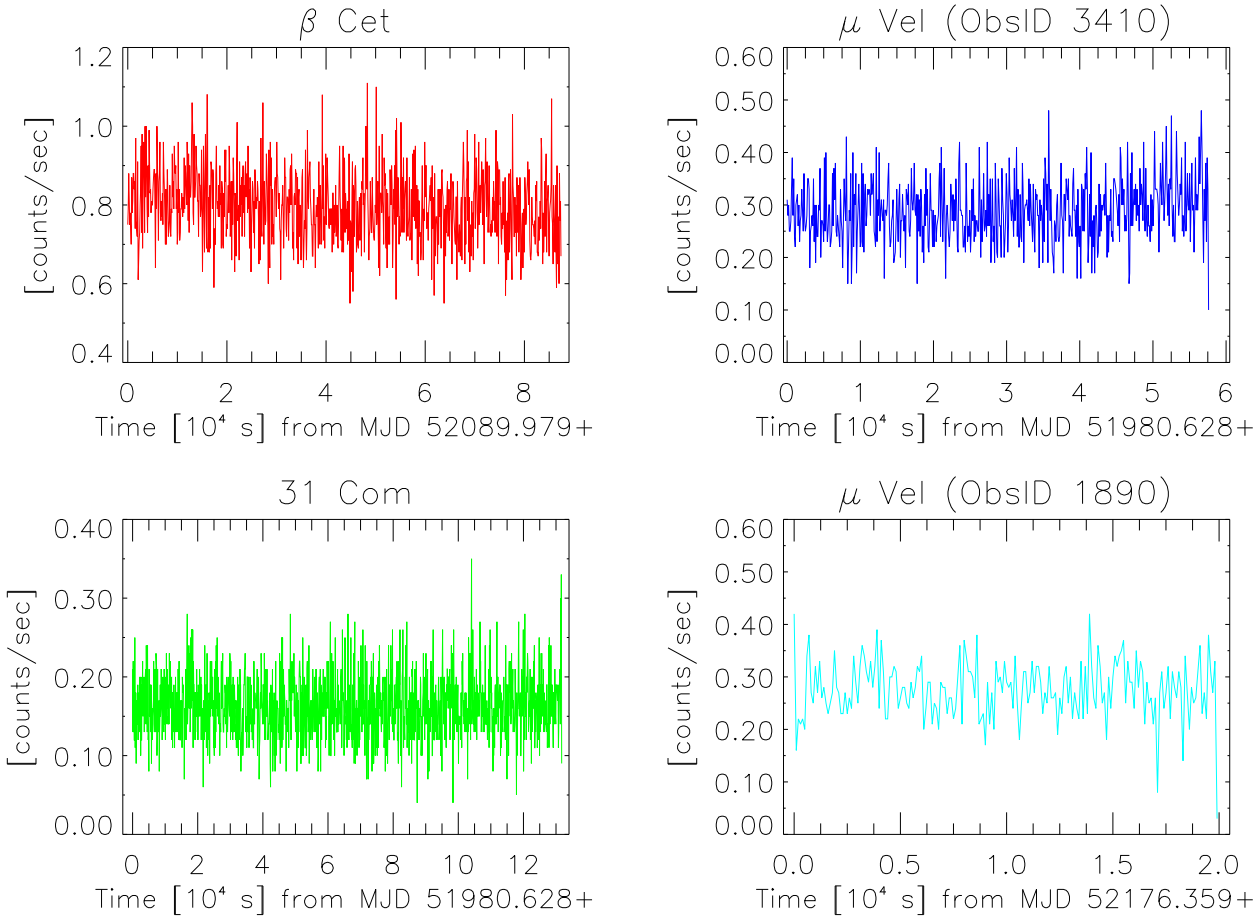

Fig. 2.— *Chandra* X-ray light curves of β Cet, 31 Com, μ Vel (ObsID 3410 and ObsID 1890). The light curves are binned at 100s intervals. All objects were relatively quiescent, showing no large flare events.

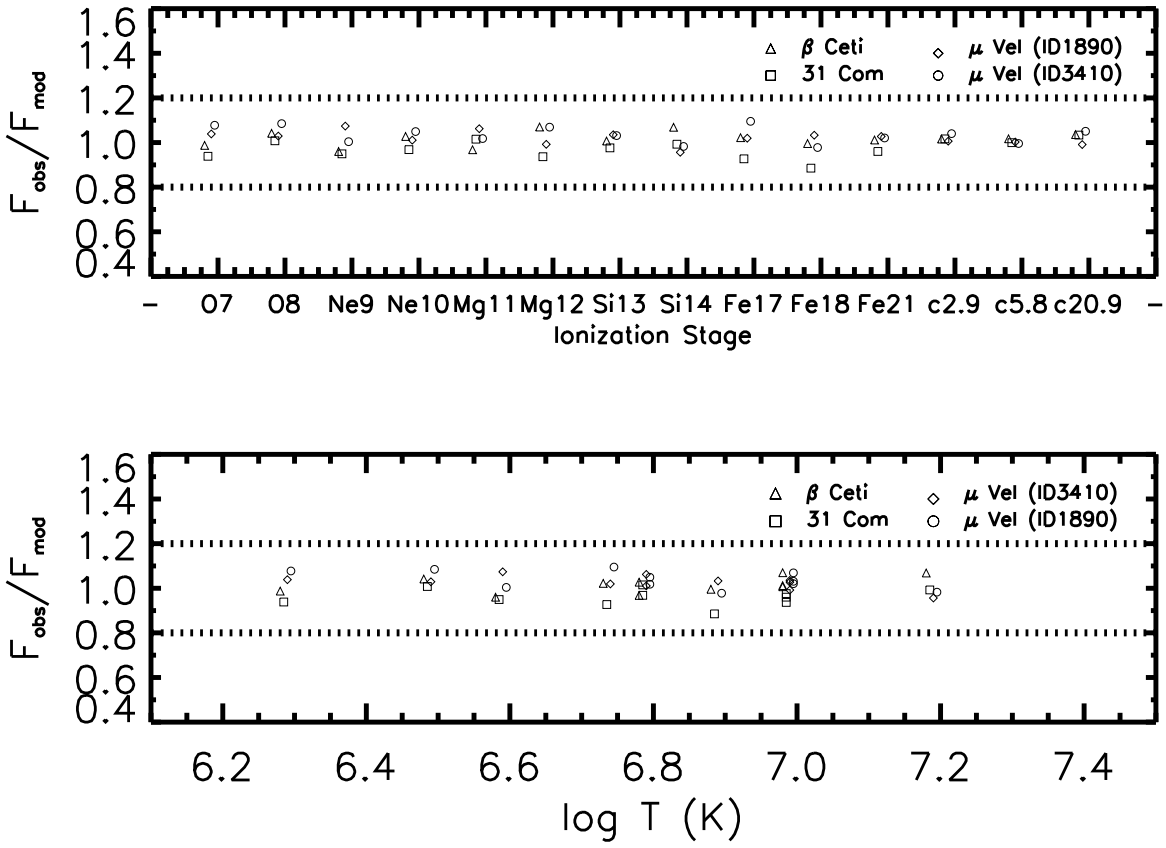

Fig. 3.— Comparison of observed and modelled line fluxes vs ionic species (upper panel) and vs T_{max} (lower panel) for β Cet, 31 Com, μ Vel (ObsID 3410 and ObsID 1890). The "line-free" continuum spectral regions at 2.4-3.4, 5.3-6.3 and 20.4-21.4 are labelled as c2.9, c5.8 and c20.9 respectively.

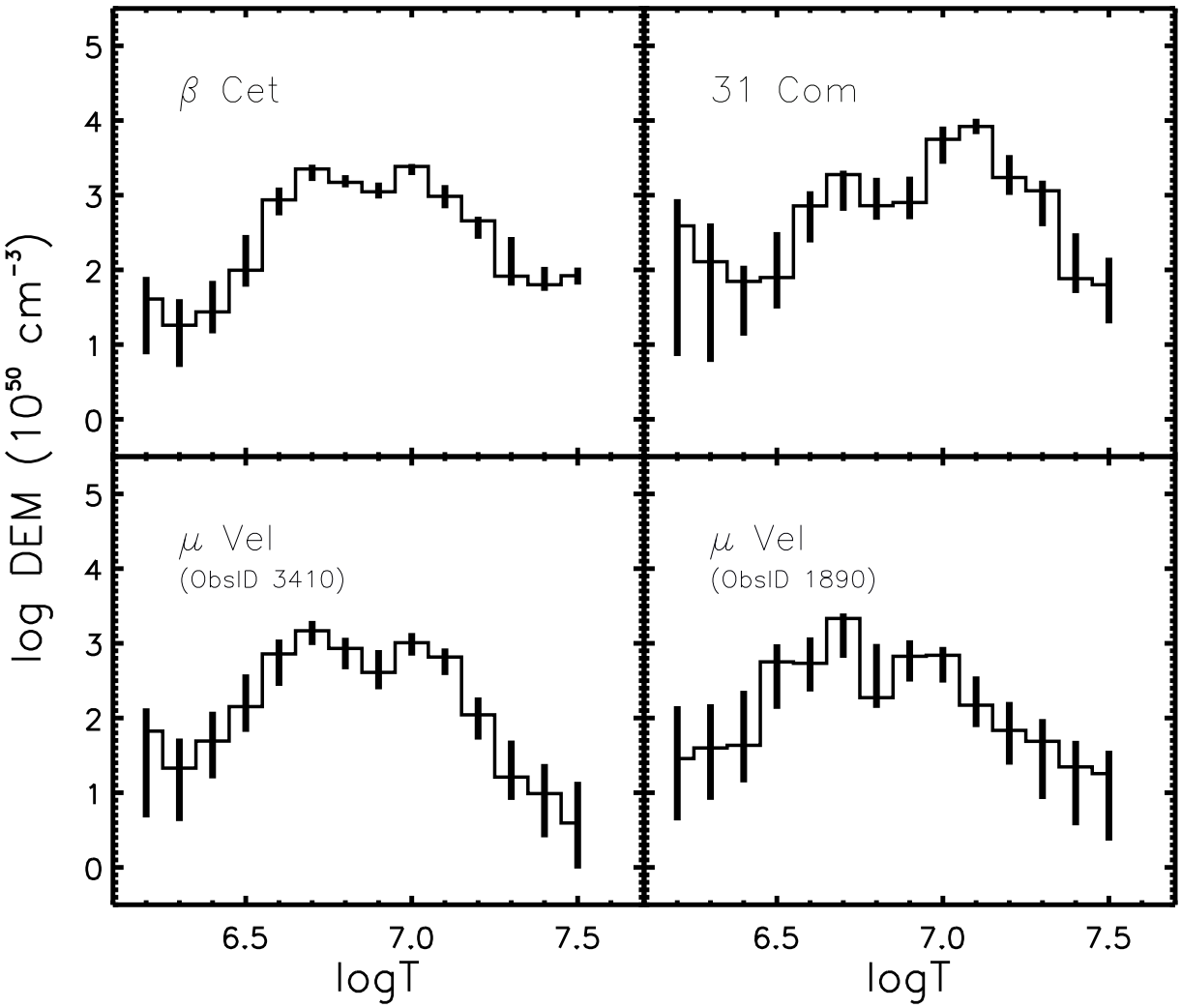

Fig. 4.— DEMs obtained for β Cet, 31 Com, μ Vel (ObsID 3410 and ObsID 1890) by running a MCMC[M] reconstruction code on a set of lines of H-like, He-like and highly ionized Fe line fluxes (O, Ne, Mg, Si, Fe XVII, Fe XVIII and Fe XXI).

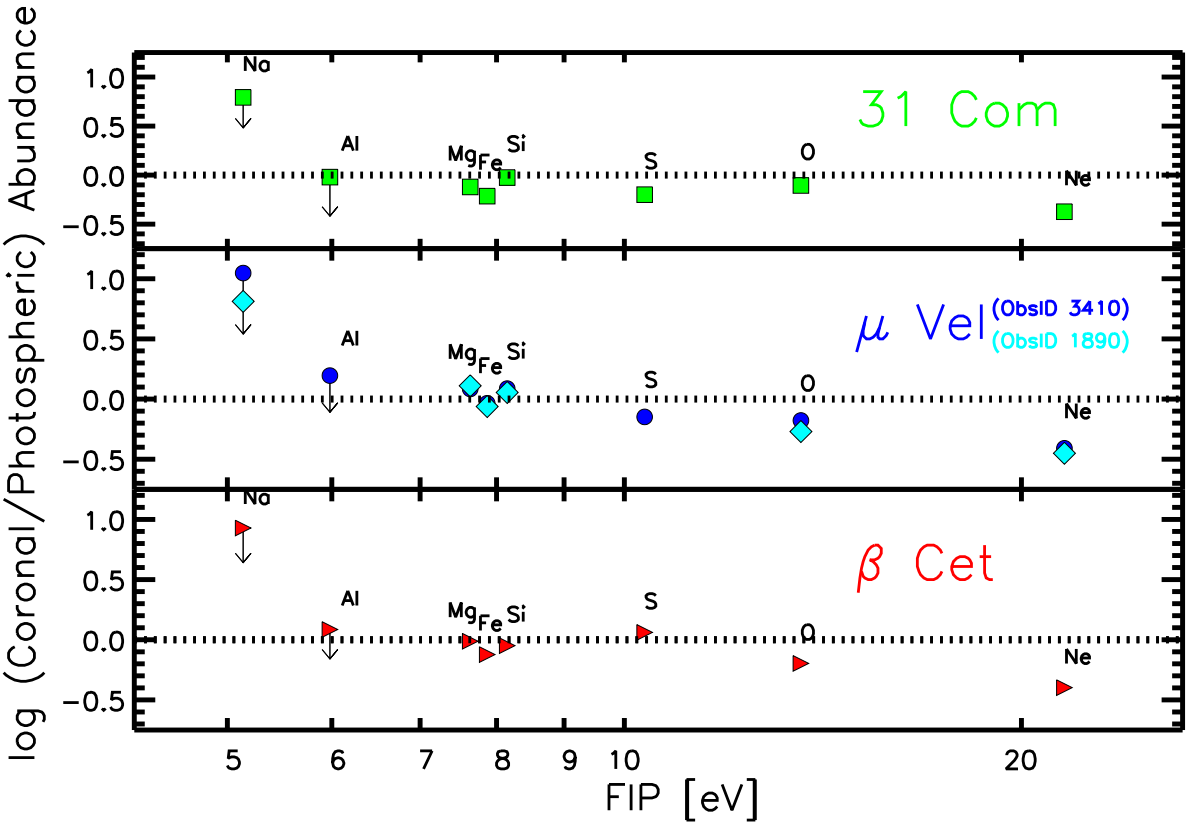

Fig. 5.— Coronal abundances obtained from abundance-insensitive DEM reconstruction for β Cet, 31 Com, μ Vel (ObsID 3410 and ObsID 1890), relative to the abundance mixture of Asplund et al. (2004) with Ne from Drake & Testa (2005) (see Table 2 and discussion in §5.2). Note: The abundances have been calculated using DEMs derived from set of ions O, Ne, Mg, Si, Fe XVII, Fe XVIII and Fe XXI for each object. The errors in the coronal abundances are ~ 0.1 dex.

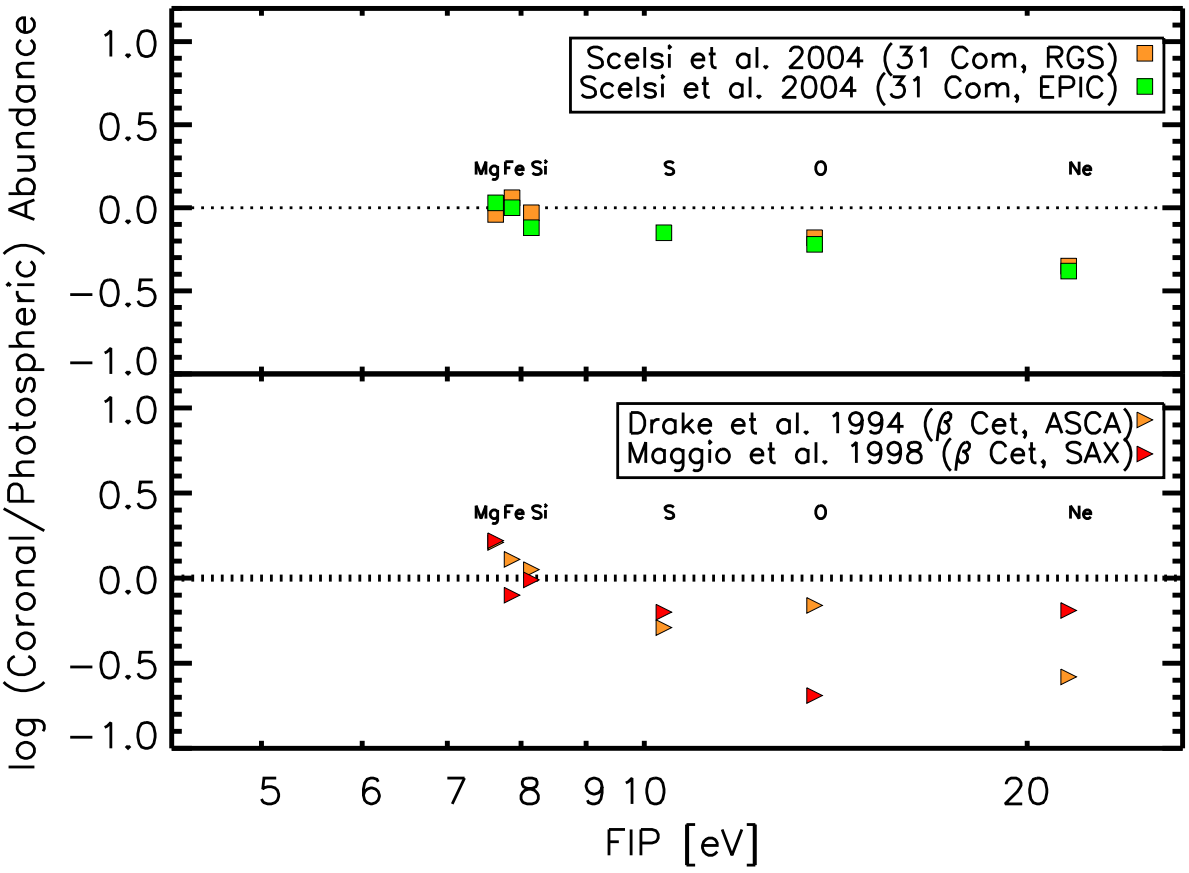

Fig. 6.— Comparison of coronal abundances against FIP for β Cet and 31 Com obtained from the literature. The values have been scaled relative to the abundance mixture of Asplund et al. (2004) with Ne from Drake & Testa (2005) (see discussion in §5.2)

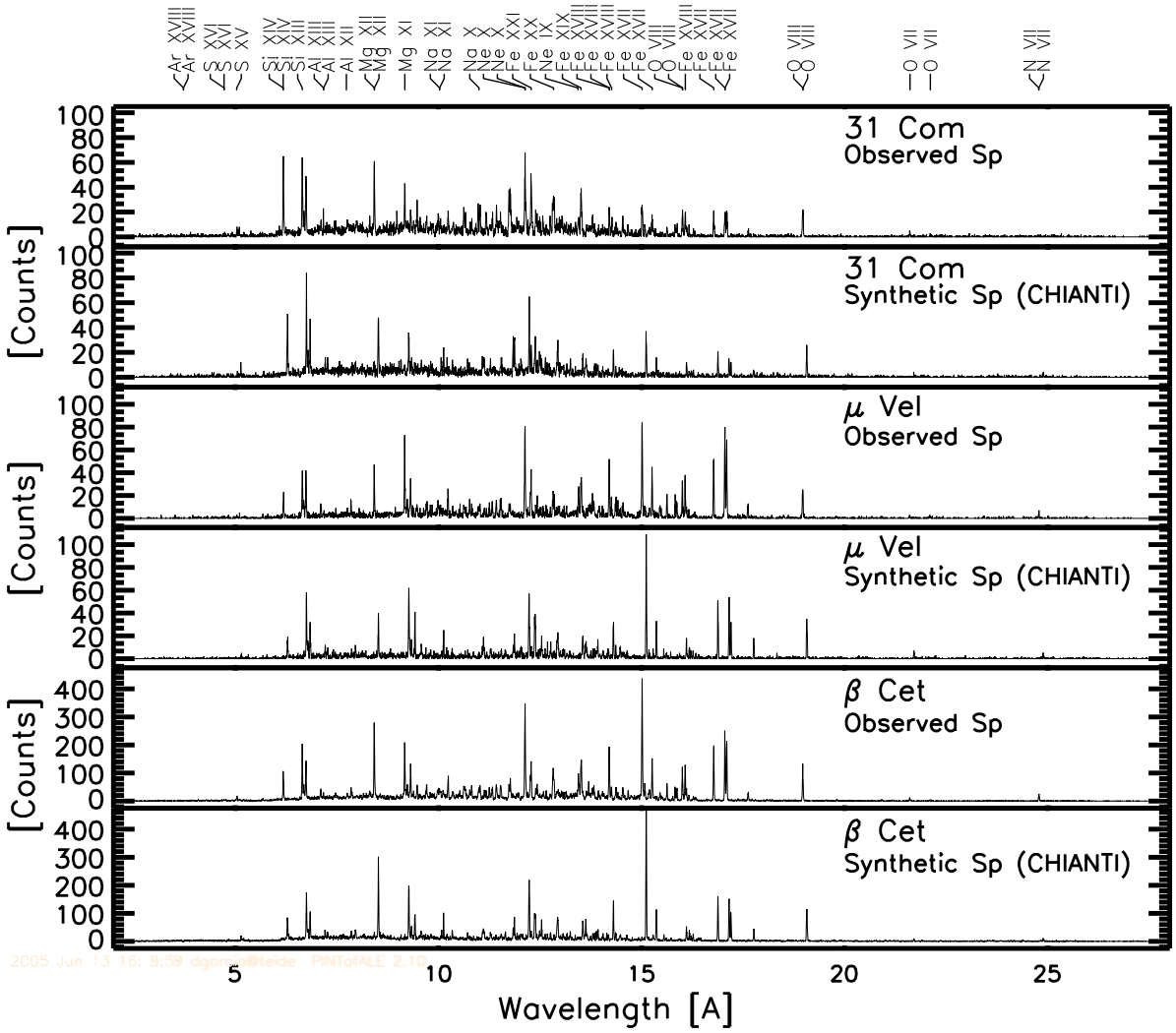

Fig. 7.— Comparison of predicted and observed HETG+ACIS-S spectra of program stars. The predicted spectra are computed using the reconstructed DEMs (see §5.1). The predicted spectrum for μ Vel is a sum of the spectra computed using the two DEMs for the two ObsIDs. The predicted spectra are offset for clarity.